Hindawi
Advances in Civil Engineering
Volume 2019, Article ID 2975274, 16 pages
https://doi.org/10.1155/2019/2975274

Research Article

Research on Mechanical Performance of CRTS III Plate-Type Ballastless Track Structure under Temperature Load Based on Probability Statistics

Zhiwu Yu,[1] Ying Xie,[2] and Xiuquan Tian[3]

[1]*Professor, National Engineering Laboratory for High Speed Railway Construction, Central South University, Changsha, China*
[2]*Ph.D. Candidate, Central South University, Changsha, China*
[3]*Central South University, Changsha, China*

Correspondence should be addressed to Ying Xie; 134801024@csu.edu.cn

Received 24 March 2019; Revised 28 May 2019; Accepted 4 June 2019; Published 26 June 2019

Academic Editor: Dimitris Rizos

CRTS III (China Railway Track System III) slab ballastless track structure is one of the high-speed railway ballastless track structures which has Chinese independent intellectual property rights. The mechanical performance of CRTS III slab ballastless track structure under temperature load has not been clear yet. Therefore, through temperature field model and temperature load values selected by statistics analysis based on long-term meteorological data, the mechanical performance of ballastless track structure is studied under two typical working conditions with different safety probability. It is found that the daily extreme values of monthly axial uniform temperature and the daily maximum temperature gradient obey certain statistical laws. In addition, the maximum tensile stress of the self-compacting concrete layer is located in the middle and edge of the slab bottom and the side of the slab. The maximum tensile stress of the base plate is located at the edge of the surface of the layer and the inner edge of the limiting groove. The interface normal tensile stress is located at the end and corner of the interface. Furthermore, maximum stress increases with the increase of safety probability.

1. Introduction

At present, high-speed railway is developing rapidly in China. Specifically, the ballastless track used in CRTS (China Railway Track System) III; is developed based on the main characteristics of that used in other ballastless track structure with certain improvements which has Chinese independent intellectual property rights. The CRTS III slab ballastless track structure consists of rail, fastening system, track slab, self-compacting concrete layer, isolation layer, bed plate, support layer, and other parts, as shown in Figure 1. Until now, in China, the total length of CRTS III slab ballastless track line under construction and operation is nearly 4000 kilometers [1]. In order to implement the strategy of China's high-speed trains going global, CRTS III slab ballastless track becomes the important technology of China's high-speed railway.

As an important environmental factor, temperature load has a significant impact on the mechanical performance and durability of slab ballastless track structure system used in high-speed railway. Therefore, the mechanical performance of ballastless track structure under temperature load has attracted the attention of many scholars. Generally, temperature load of ballastless track structure mainly includes axial uniform temperature and temperature gradient. China's high-speed railway design specification stipulated in the temperature gradient is 45°C/m. Many scholars and research institutions took some temperature tests on ballastless track structure and found that the track plate temperature gradient was between 40~80°C/m, maximum negative temperature gradient is half of the maximum positive temperature gradient, and the temperature change of the bed plate is not obvious [2–5]. The long-term observation of ballastless track structure shows that the

Figure 1: The composition of CRTS III slab ballastless track structure.

temperature field inside ballastless track structure is mainly affected by solar radiation, wind speed, and atmospheric temperature and varied on a daily basis with temperature, and the vertical temperature presents a nonlinear distribution [6–11]. With the increase of depth, the amplitude of temperature change in ballastless track structure decreases and the peak value lags [12–16]. The study in literature [17] further shows that both positive and negative temperature gradients show nonlinear distribution and their occurrence time is basically equal.

However, these studies are generally based on the specific environment or special working conditions which the values of various parameters are not standardized and unified. Therefore, it is necessary to determine the appropriate temperature load first, and then study the mechanical performance of CRTS III plate-type ballastless track structure system under the temperature load.

2. Temperature Field Model of Ballastless Track Structure

As a multilayer structure, the temperature change in the CRTS III slab ballastless track structure caused by the change of the external environment is mainly concentrated in the position shallower from the surface [10]. Therefore, considering that the boundary condition does not change along the track longitudinal, the calculation of temperature field of ballastless track can be simplified to the solution of a one-dimensional differential equation of heat conduction. When the temperature changes harmonically on the structure surface, the temperature field inside ballastless track structure can be regarded as the superposition of temperature inside the plate which was caused by the action of atmospheric temperature θ_a and equivalent temperature increment $\Delta\theta$, respectively, which is given as follows:

$$\theta(x,t) = \theta_{ac}(x,t) + \Delta\theta_c(x,t). \tag{1}$$

In addition, the temperature variation within the structure $\theta_{ac}(x,t)$ coursed by the change of atmospheric temperature θ_a can be shown as follows:

$$\theta_{ac}(x,t) = \begin{cases} \theta_{ave} + \theta_{amp} e^{-x\sqrt{\pi/2\alpha T}} \cos\left(\dfrac{\pi}{T}t - \dfrac{T+T_{min}}{T}\pi - x\sqrt{\dfrac{\pi}{2\alpha T}}\right), & T_{min} \le t < T_{min} + T, \\ \theta_{ave} + \theta_{amp} e^{-x\sqrt{\pi/(2\alpha(24-T))}} \cos\left(\dfrac{\pi}{24-T}t - \dfrac{T+T_{min}}{24-T}\pi - x\sqrt{\dfrac{\pi}{2\alpha(24-T)}}\right), & T_{min} + T \le t < T_{min} + 24, \end{cases} \tag{2}$$

where θ_{ave} denotes mean value of daily temperature variation, θ_{amp} denotes daily temperature variation, and T_{min} denotes the moment of the lowest temperature in a day.

And the temperature variation within the structure $\Delta\theta_c(x,t)$ coursed by the change of equivalent temperature increment $\Delta\theta$ can be shown as follows:

$$\Delta\theta_c(x,t) = \frac{\pi A_s I}{2t_{day}h_{cr}} e^{-x\sqrt{\pi/2\alpha t_{day}}} \cos\left[\frac{\pi}{t_{day}}(t-12) - x\sqrt{\frac{\pi}{2\alpha t_{day}}}\right], \quad T_{min} + \Delta\varphi \le t \le t_{day} + T_{min} + \Delta\varphi,$$
$$\Delta\varphi = \frac{x t_{day}}{\pi}\sqrt{\frac{\pi}{2\alpha t_{day}}}, \tag{3}$$

where A_s denotes absorptance for solar radiation which ranges from 0.5 to 0.7 for concrete, I denotes the daily amount of solar radiation received by the surface of the structure, h_{cr} denotes surface thermal conductance, 19 W/(m^2·°C), t_{day} denotes daylength αdenotes thermal diffusion coefficient, 0.00313 m^2/s, x denotes the distance to the surface of the structure, and t denotes a certain time in daytime.

3. Temperature Load Values Selected Based on Probability and Statistics

Literature [18] stipulates that the effect of the change of axial uniform temperature and temperature gradient should be taken into account in the ordinary size concrete beam and slab. For ballastless track structure, due to the periodicity and regularity of the daily internal temperature field, the axial uniform temperature and temperature gradient reflected by it have a similar periodicity and regularity. In order to study the mechanical properties of CRTS III slab ballastless track structure under temperature load, it is necessary to describe this periodicity and regularity statistically.

3.1. Temperature Load Extremum Probability Model. In order to describe the temperature load of ballastless track structure, it can be transformed into a random process, and then according to the sample function of the load or the existing load distribution characteristics, the maximum value of the load in the design reference period is determined. The specific steps are as follows:

(i) The design reference period of ballastless track structure is determined to be T years.

(ii) According to the periodicity and regularity of temperature change in a certain area, the design reference period can be divided into N periods (τ_i), which can be shown as follows: $T = \sum_{i=1}^{N} \tau_i$.

(iii) The distribution function ($F_{\tau_i,\max}(x)$) of the maximum value of load ($Q_{i,\max}$) within the time period (τ_i) was obtained by statistics. The distribution function of the maximum load in each time period is the same and independent. Therefore, the maximum temperature load in the design reference period can be shown as follows:

$$Q_{T,\max} = \max\left\{Q_{1,\max}, Q_{2,\max}, \ldots, Q_{N,\max}\right\}. \quad (4)$$

And its distribution function can be shown as follows:

$$P\left(Q_{N,\max} \le x\right) = \left[F_{\tau_i,\max}(x)\right]^N. \quad (5)$$

Similarly, the minimum load and its distribution in the design reference period can be obtained:

$$Q_{T,\min} = \min\left\{Q_{1,\min}, Q_{2,\min}, \ldots, Q_{N,\min}\right\},$$
$$P\left(Q_{N,\max} > x\right) = 1 - \left[1 - F_{\tau_i,\min}(x)\right]^N. \quad (6)$$

Based on the time period probability distribution ($F_{\tau_i}(x)$) and its statistical parameters, the distribution ($F_{\tau_i,\max(\min)}(x)$) of the maximum (minimum) load ($Q_{\tau_i,\max(\min)}$) and its statistical parameters in the design reference period can be obtained according to the above formula.

3.2. Statistical Analysis of Axial Uniform Temperature. Since the CRTS III slab ballastless track structure used in this research relies on the Zhengzhou-Xuzhou passenger dedicated line, in order to be more representative, the meteorological data (maximum and minimum temperatures and solar radiation intensity) of every day in Zhengzhou from 2008 to 2017 were counted, and then the daily value of axial uniform temperature of ballastless track structure was calculated. However, it is difficult to obtain the distribution law of the diurnal extreme value of the axial uniform temperature in the past ten years. Considering that the temperature of the same month is basically similar in different years, the frequency histogram of the days with different extreme temperature values was obtained by taking the months of different years as the statistical period, which for some months are shown in Figures 2–5.

It can be seen from Figures 2–5 that the daily extreme values of monthly axial uniform temperature of CRTS III slab ballastless track structure in Zhengzhou show a trend of normal distribution, which can be fitted by using the normal distribution function. Furthermore, by using the Jarque–Bera test function in Matlab, the goodness of fit test of normal distribution was carried out which the significance level α was 5%, as shown in Figures 6–9. The estimated values of the normal distribution parameters of the daily extreme values of the axial uniform temperature in different months are shown in Table 1.

According to the parameter estimation of the daily maximum distribution function of axial uniform temperature of ballastless track structure in different months, the probability distribution function of axial uniform temperature in different months in Zhengzhou can be obtained as follows:

$$F_{\tau-m,i}(x) = \frac{1}{\sqrt{2\pi}\sigma_i} \int_{-\infty}^{x} e^{\left((x-\mu_i)^2\right)/2\sigma_i^2} dx. \quad (7)$$

It is considered that the daily distribution of axial uniform temperature of ballastless track structure in each month is independent from each other. Therefore, the annual probability distribution function of the daily extreme value of the axial uniform temperature is shown as follows:

$$F_{\tau-y,i}(x) = \omega_1 F_{\tau-m,1}(x) + \omega_2 F_{\tau-m,2}(x) + \cdots + \omega_{12} F_{\tau-m,12}(x), \quad (8)$$

where $F_{\tau-m,i}(x)$ denotes the probability distribution function of the daily extreme value of axial uniform temperature of ballastless track structure of ith month in a year. $F_{\tau-y,i}(x)$ denotes the annual probability distribution function of the daily extreme value of the axial uniform temperature. ω_i denotes the weight coefficient which can be 1/12.

The daily extreme distribution of axial uniform temperature of ballastless track structure in the design reference period is shown as follows:

$$\begin{aligned} F_{T,\max}(x) &= \left[\omega_1 F_{\tau-m,1}(x) + \omega_2 F_{\tau-m,2}(x) + \cdots \right. \\ &\quad \left. + \omega_{12} F_{\tau-m,12}(x)\right]^N, \\ F_{T,\min}(x) &= 1 - \left\{1 - \left[\omega_1 F_{\tau-m,1}(x) + \omega_2 F_{\tau-m,2}(x) + \cdots \right.\right. \\ &\quad \left.\left. + \omega_{12} F_{\tau-m,12}(x)\right]\right\}^N. \end{aligned} \quad (9)$$

The base design period of high-speed railway is 60 years in China. Therefore, the corresponding axial uniform temperature can be obtained by different safety probability percentages such as 50%, 90%, and 95%, as shown in Table 2.

3.3. Statistical Analysis of Temperature Gradients. The daily maximum temperature gradient of CRTS III slab ballastless track structure was calculated and analyzed to obtain the histograms which are shown in Figure 10. As can be seen from Figure 10, the daily maximum temperature gradient of ballastless track structure presents an obvious skewed distribution and tends to the extreme value I-type distribution:

$$F_\tau(x) = \exp\left[-\exp\left(-\frac{x-\beta}{\alpha}\right)\right],$$
$$\begin{cases} \alpha = \dfrac{\sigma}{1.2826}, \\ \beta = \mu - 0.5772\alpha. \end{cases} \quad (10)$$

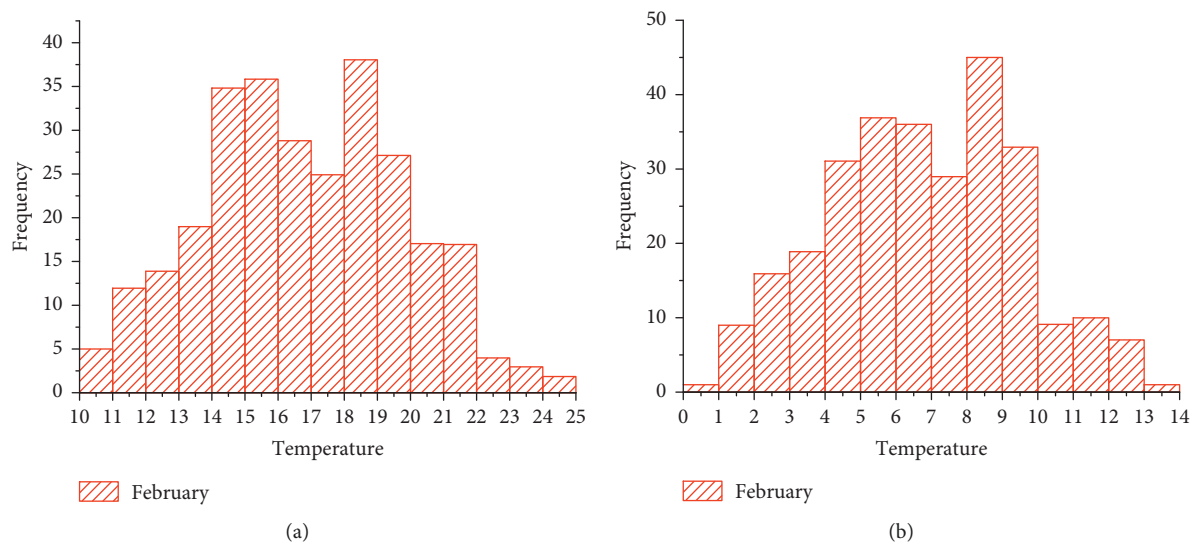

Figure 2: The histogram of the daily extreme value of axial uniform temperature in February. (a) The maximum. (b) The minimum.

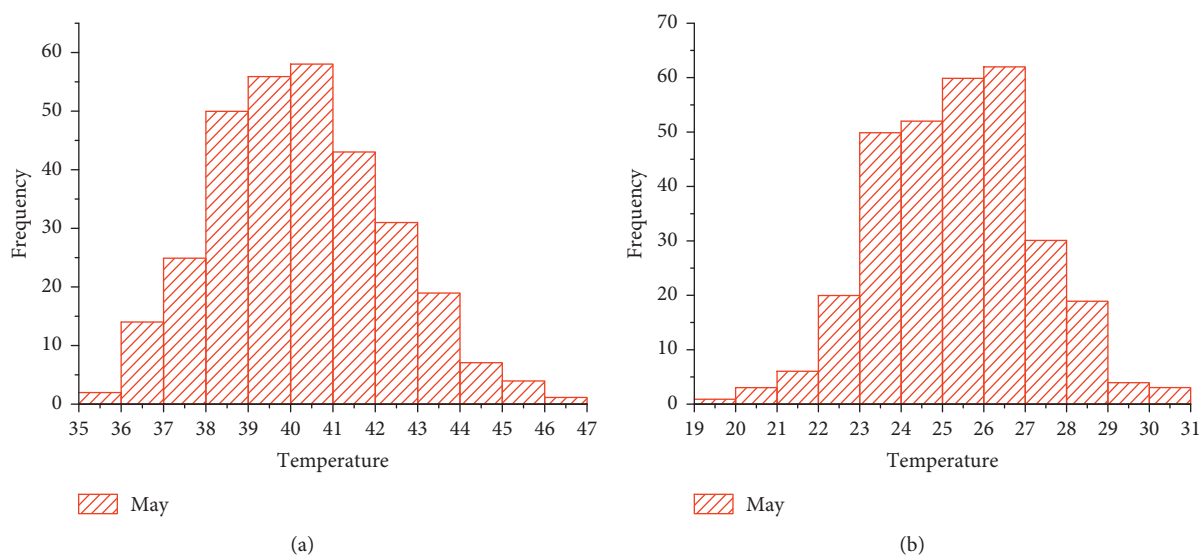

Figure 3: The histogram of the daily extreme value of axial uniform temperature in May. (a) The maximum. (b) The minimum.

Therefore, the statistical parameters of the daily maximum annual distribution of temperature gradient of CRTS III plate-type ballastless track structure in Zhengzhou can be fitted, as shown in Table 3.

The base design period of high-speed railway is 60 years in China. Therefore, the corresponding temperature gradients can be obtained by calculating the safety probability percentages such as 50%, 90%, and 95%, as shown in Table 4.

4. Finite Element Model of Ballastless Track Structure

4.1. The Selection of Parameters. In the finite element (FE) model, the main structure components of CRTS III slab ballastless track system consist of rail, track board, self-compacting concrete (SCC) layer, isolation layer, bed pate, and other parts. Geometric parameters and material parameters of components are selected according to the relevant literature [19], which are listed in Table 5.

4.2. The Selection of Constitutive Models. In this work, the constitutive models selection of concrete and steel bars is the same as the literature [20]. The constitutive models of concrete can be shown as follows:

$$\sigma_n = [I - D(n)]E_0\varepsilon_n, \tag{11}$$

where σ_n denotes the effective stress. ε_n denotes the total strain, and E_0 represents initial Young's modulus. $D(n)$ denotes the damage variable.

The constitutive models of steel bars can be shown as follows:

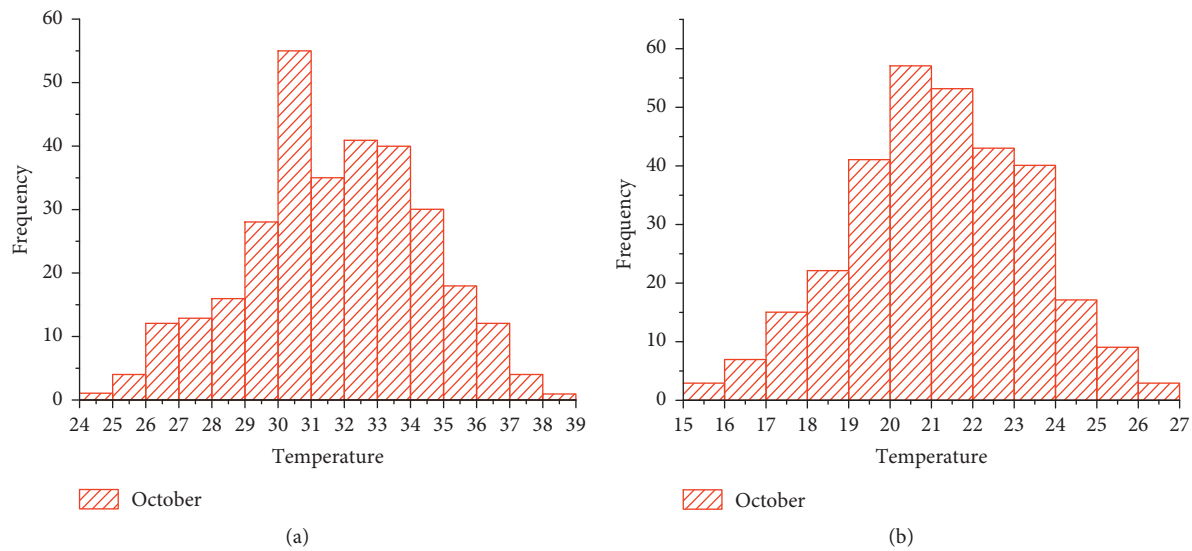

Figure 4: The histogram of the daily extreme value of axial uniform temperature in October. (a) The maximum. (b) The minimum.

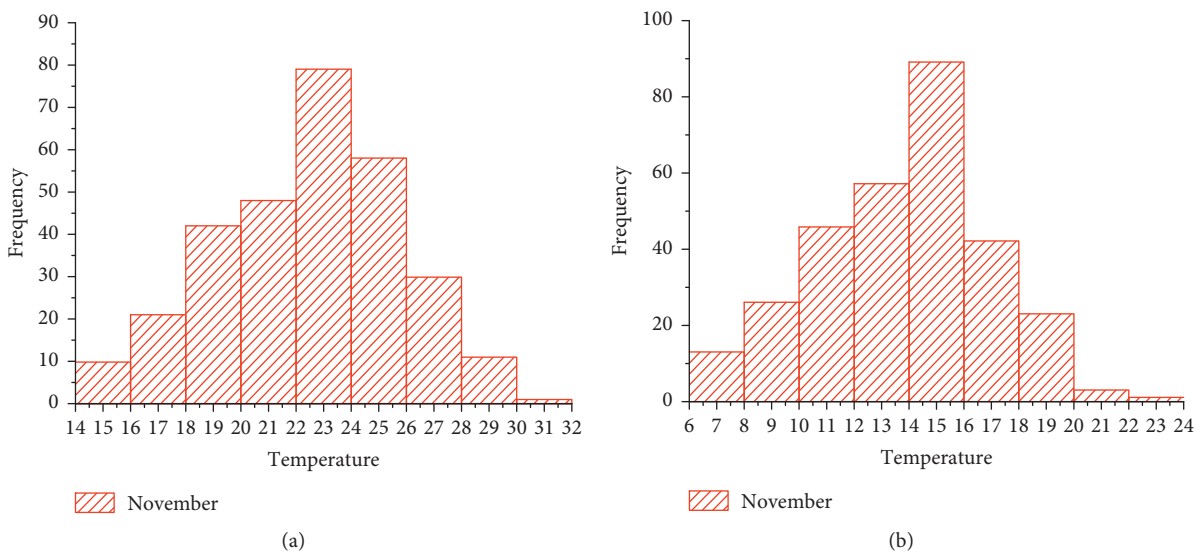

Figure 5: The histogram of the daily extreme value of axial uniform temperature in November. (a) The maximum. (b) The minimum.

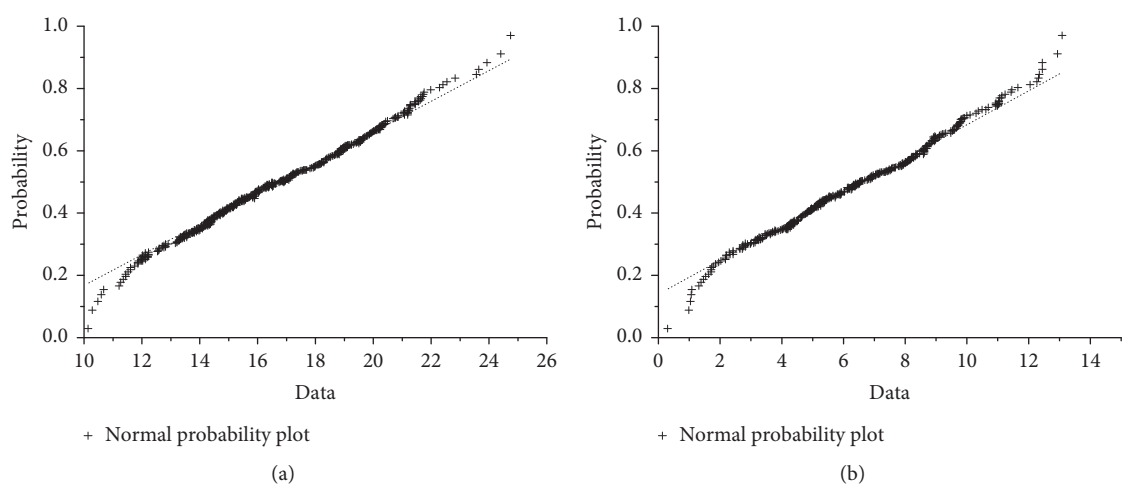

Figure 6: The distribution probability diagram of the daily extreme value of axial uniform temperature in February. (a) The maximum. (b) The minimum.

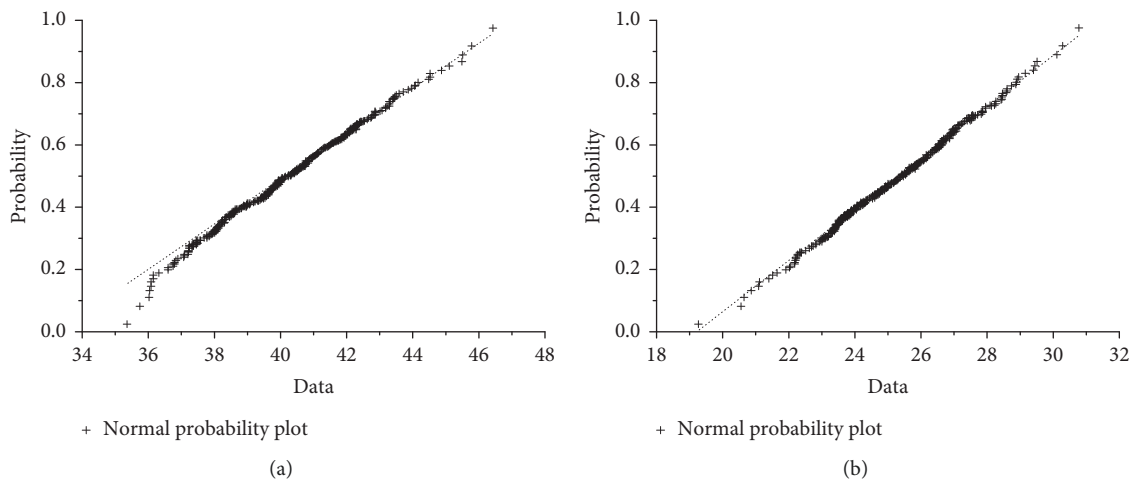

Figure 7: The distribution probability diagram of the daily extreme value of axial uniform temperature in May. (a) The maximum. (b) The minimum.

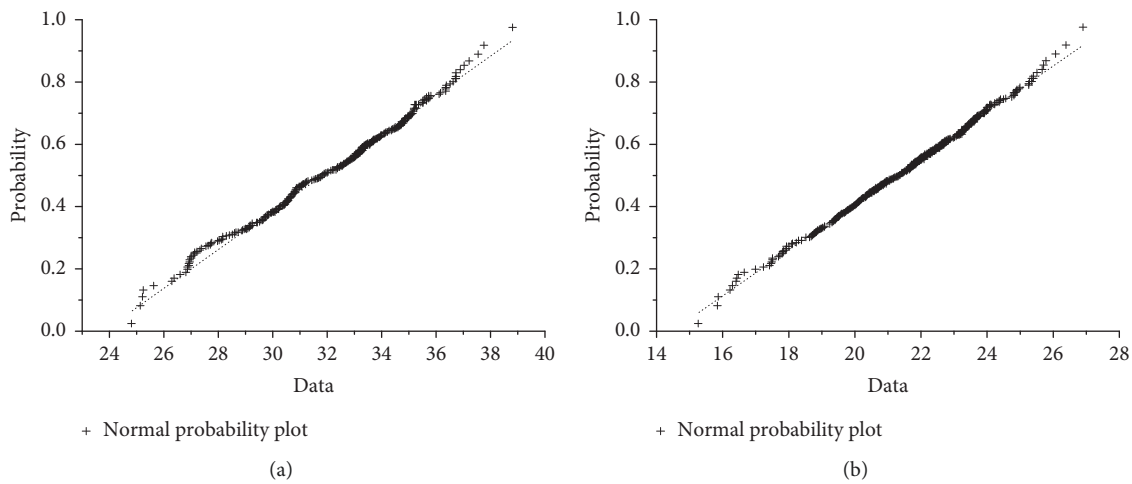

Figure 8: The distribution probability diagram of the daily extreme value of axial uniform temperature in October. (a) The maximum. (b) The minimum.

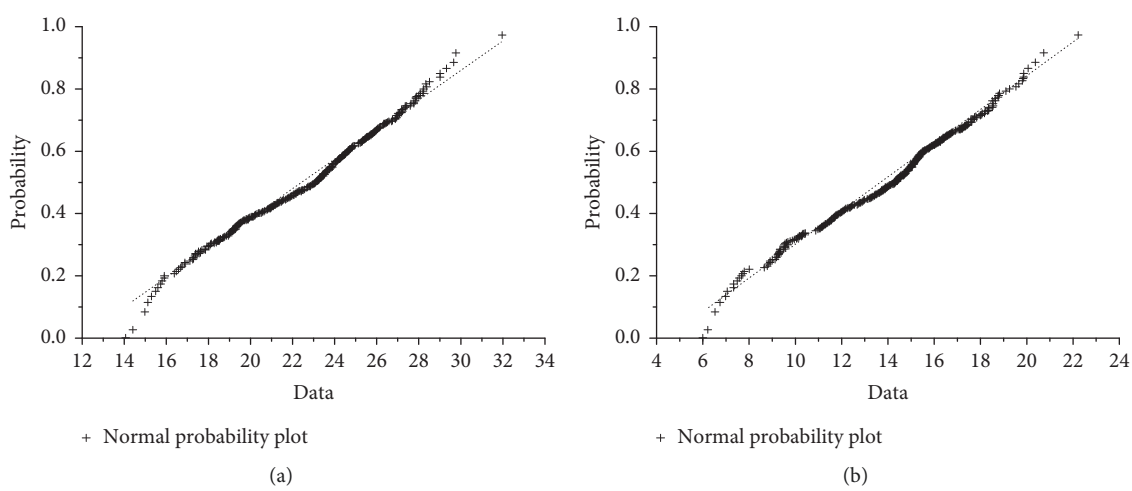

Figure 9: The distribution probability diagram of the daily extreme value of axial uniform temperature in November. (a) The maximum. (b) The minimum.

Table 1: The estimated values of the normal distribution parameters of the daily extreme values of the axial uniform temperature in different months.

	Months	1	2	3	4	5	6	7	8	9	10	11	12
The maximum	μ	12	17	25	33	40	44	48	47	40	32	23	15
	σ	2.5	3.0	3.3	3.0	2.1	1.8	2.1	2.3	2.4	2.7	3.3	2.5
The minimum	μ	3.6	6.8	12	19	25	29	33	33	28	21	14	6.7
	σ	2.4	2.7	2.7	2.6	1.9	1.6	2.0	1.9	2.0	2.2	3.1	2.5

Table 2: Axial uniform temperature based on different safety probability percentages.

	$T = 60$ years		
Safety probability (%)	$P = 50$	$P = 90$	$P = 95$
The maximum (°C)	50.6544	52.4781	53.0506
The minimum (°C)	0.7437	−1.3437	−1.9973

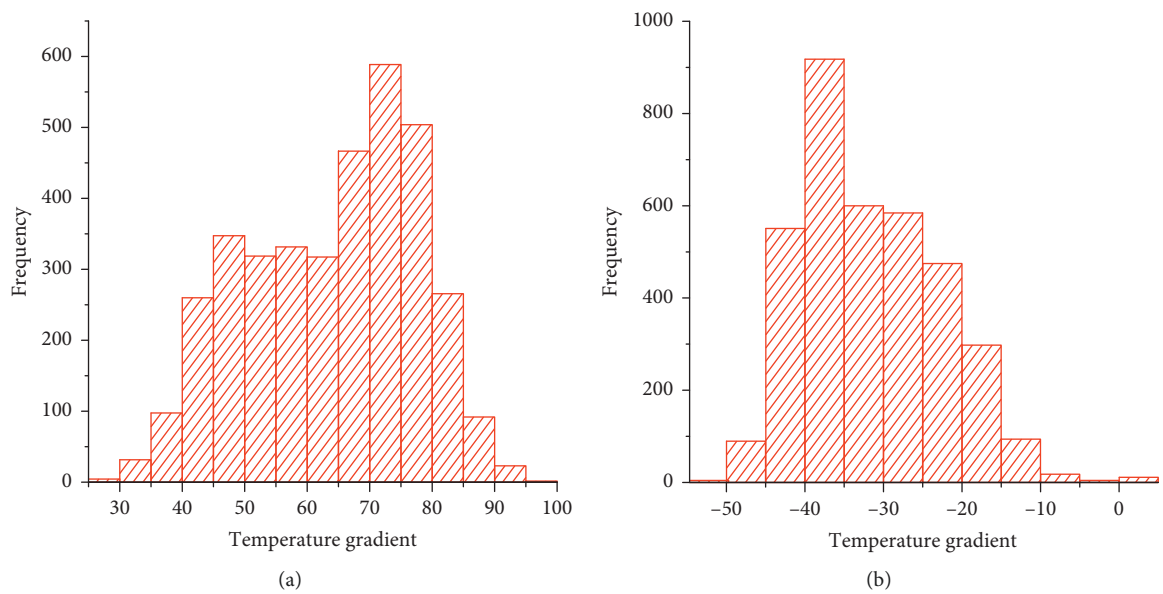

Figure 10: Histogram of daily maximum frequency of temperature gradient. (a) Positive temperature gradient. (b) Negative temperature gradient.

Table 3: The statistical parameters of the daily maximum annual distribution of temperature gradient.

	A	β
Positive temperature gradient	11.8	70.5
Negative temperature gradient	7.3	35.8

Table 4: Temperature gradient daily maximum load based on different safety probability percentages.

	$T = 60$ years		
Safety probability (%)	$P = 50$	$P = 90$	$P = 95$
Positive temperature gradient (°C/m)	88.2	92.3	93.6
Negative temperature gradient (°C/m)	46.7	49.3	50.1

Table 5: The basic specifications of main members.

	Rail	Track slab	Self-compacting concrete layer	Bed plate	Isolation layer	Support layer
Length (mm)		5600	5600	5600	5600	
Width (mm)		2500	2500	2900	2600	
Height (mm)		200	90	200	4	
Concrete strength		C60	C40	C30		
Elasticity modulus	210 GPa	36000 MPa	34000 MPa	32000 MPa	3.32 MPa	
Poisson's ration	0.3	0.2	0.2	0.2	0.35	
Thermal expansion coefficient ($^{\circ}C^{-1}$)	1.18×10^{-5}	1×10^{-5}	1×10^{-5}	1×10^{-5}		1×10^{-5}
Stiffness						1000 MPa/m
Density	7800 kg/m^3	2500 kg/m^3	2500 kg/m^3	2500 kg/m^3	700 g/m^2	

$$f_y(N) = (\sigma_{\min} + \Delta\sigma)\left[1 - \frac{\lg N}{\lg N_f}\left(1 - \frac{\sigma_{\min} + \Delta\sigma}{f_y}\right)\right],$$
$$\sigma(N) = \begin{cases} E_s\varepsilon(N), & \Delta\varepsilon_r(N-1) < \varepsilon(N) \le \varepsilon_y(N), \\ f_y(N), & \varepsilon(N) > \varepsilon_y(N), \end{cases}$$
$$\varepsilon_r(N) = \Delta\varepsilon_r(N-1) + \frac{f_y}{E_s},$$
$$\Delta\varepsilon_r(N-1) = \frac{\left[f_y(N) - f_y(N-1)\right]}{E_s}, \tag{12}$$

where E_s denotes the initial Young's modulus of rebar. f_y and $f_y(N)$ denote the initial yield strength and yield strength after N times fatigue load. $\varepsilon_r(N)$ and $\Delta\varepsilon_r(N)$ denote the yield strain and residual strain after N times fatigue load.

4.3. Development of FE Model of CRTS III Slab Ballastless Track Structure. The FE model of the CRTS III slab ballastless track system is developed on the commercial software ANSYS, as shown in Figure 11. The FE units of main structural layers are determined as shown in Table 6. In addition, the interfaces between slabs should be considered. The interfaces between track slab and self-compacting concrete layer can be modelled by cohesive elements. And the interfaces between self-compacting concrete layer and isolation layer and the interfaces between isolation layer and bed plate can be modelled by contact interface element with detailed parameters determined based on the internal frictional force of these two interfaces [21].

Additionally, the slab ballastless track structure was consolidated with the support layer simulated by using the spring element in which all degrees of freedom of the lower node are constrained. The degrees of freedom in two horizontal directions of the bed plate are constrained, and all degrees of freedom of the rail are constrained. Furthermore, all degrees of freedom at both ends of the rail are constrained.

4.4. Model Verification. He [22] studied the deformation behavior of the CRTS III slab ballastless track system under the temperature effect on the rigid support. Research shows that under the action of 100°C/m temperature gradient, the maximum displacement of track plate relative to the base plate is 0.951 mm which located at the angle of plate. Furthermore, under the action of −20°C/m temperature gradient, the maximum displacement of the track plate relative to the base plate is 0.180 mm which also located at the angle of plate.

Based on the FE model, calculate the deformation of CRTS III slab ballastless track under the same condition as that in literature [22], as shown in Figures 12 and 13. The maximum displacement of the track plate relative to the base plate is 0.861 mm under the action of 100°C/m temperature gradient, which is 9.5% smaller than the measured value in reference literature [22]. In addition, the maximum displacement of the track plate relative to the base plate is 0.192 mm under the action of −20°C/m temperature gradient, which is 3.2% smaller than the measured value in reference literature [22]. Therefore, the FE model proved to be reasonable and reliable.

5. Mechanical Performance of Key Structural Layers of Ballastless Track Structure

Generally, in the track system, due to the high strength of the concrete material and the two-dimensional prestressing structure used in the track board, the self-compacting concrete layer and bed plate are required to be carefully examined on the performance under the temperature loading. There are two conditions that apply to the FE model: condition 1 (the daily maximum value of axial uniform temperature is combined with the daily maximum value of the positive temperature gradient) and condition 2 (the daily minimum value of axial uniform temperature is combined with the daily maximum value of the negative temperature gradient).

5.1. Stress Condition of Self-Compacting Concrete Layer. Under condition 1, the stress of the self-compacting concrete layer is shown in Figures 14 and 15. The maximum longitudinal tensile stress of the self-compacting concrete layer is located in the middle of the bottom surface and the side of this layer. The maximum transverse tensile stress is located at the bottom edge of the layer and the side of the layer. Furthermore, the maximum stress increases with the increase of the fractal value.

Under condition 2, the stress of the self-compacting concrete layer is shown in Figures 16 and 17. The maximum

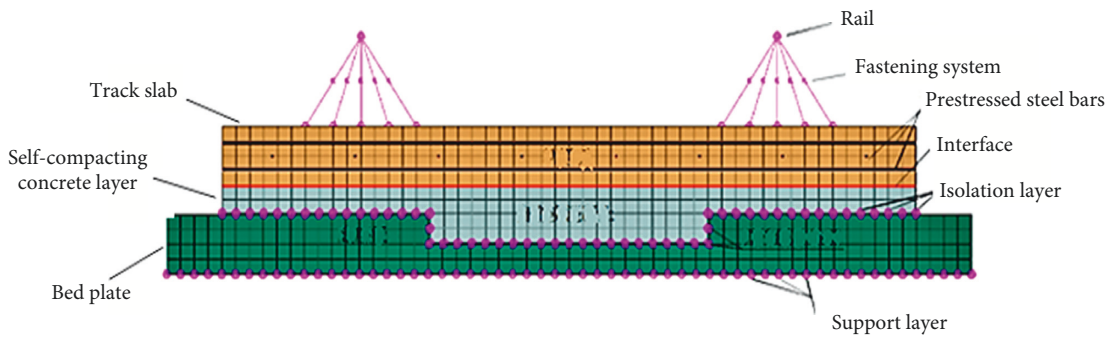

Figure 11: The finite element model of the CRTS III slab ballastless track system.

Table 6: The finite element units of main structural layers.

Structural layers	Finite element units
Concrete	Solid 65
Rail	Beam 188
Support layer	Combin 14
Fastening system	Combin 14
Isolation layer	Solid 45
Interface between track slab and SCC layer	Inter205
Interface between isolation layer and SCC layer	Target 170
Interface between isolation layer and bed plate	Target 170

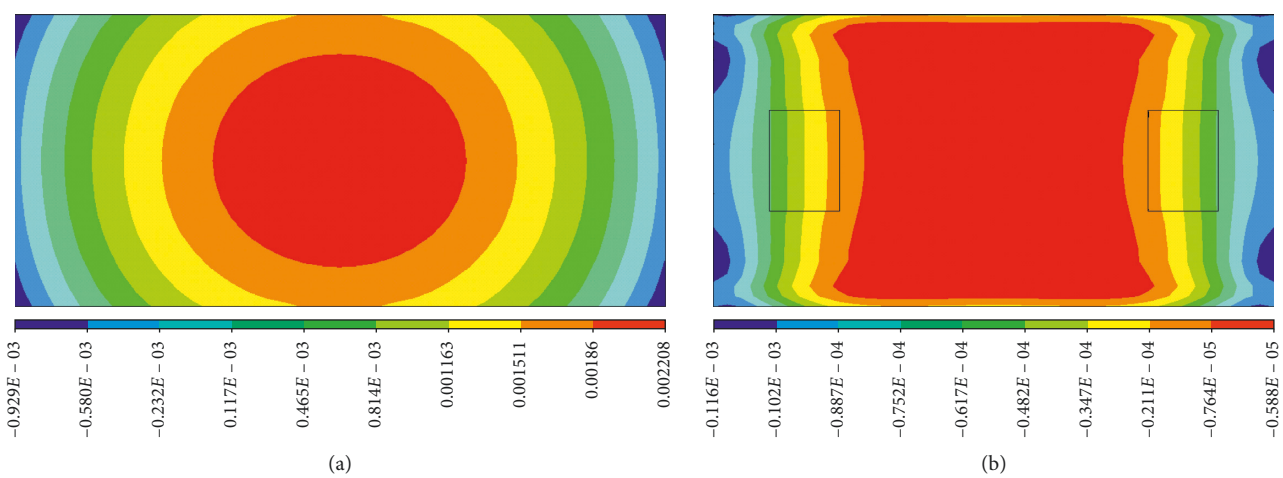

Figure 12: The deformation under 100°C/m temperature gradient. (a) Track slab. (b) Bed plate.

longitudinal tensile stress of the self-compacting concrete layer is located at the side of the layer and the maximum transverse tensile stress is located at the bottom edge of the layer. In addition, the maximum longitudinal tensile stress increases with the increase of the fractal value, but the maximum transverse tensile stress remained basically stable. Furthermore, both longitudinal and transverse maximum compressive stress decreases slightly with the increase of the fractal value, as shown in Table 7.

5.2. Stress Condition of Bed Plate. Under condition 1, the stress of the bed plate is shown in Figures 18 and 19. The maximum longitudinal tensile stress of the bed plate is located at both ends of the bottom surface of the layer and the inner edge of the limiting groove. The maximum transverse tensile stress is located at the side of the layer and the inner edge of the limiting groove. Under condition 2, the stress of the bed plate is shown in Figures 20 and 21. Both longitudinal and transverse maximum tensile stresses are located at the edge of the upper surface of the base plate. Furthermore, the maximum stress increases with the increase of the fractal value, as shown in Table 8.

5.3. Stress Condition of Interface between Track Slab and Self-Compacting Concrete Layer. Under condition 1, the stress of interface between track slab and self-compacting concrete layer is shown in Figures 22 and 23. The maximum normal

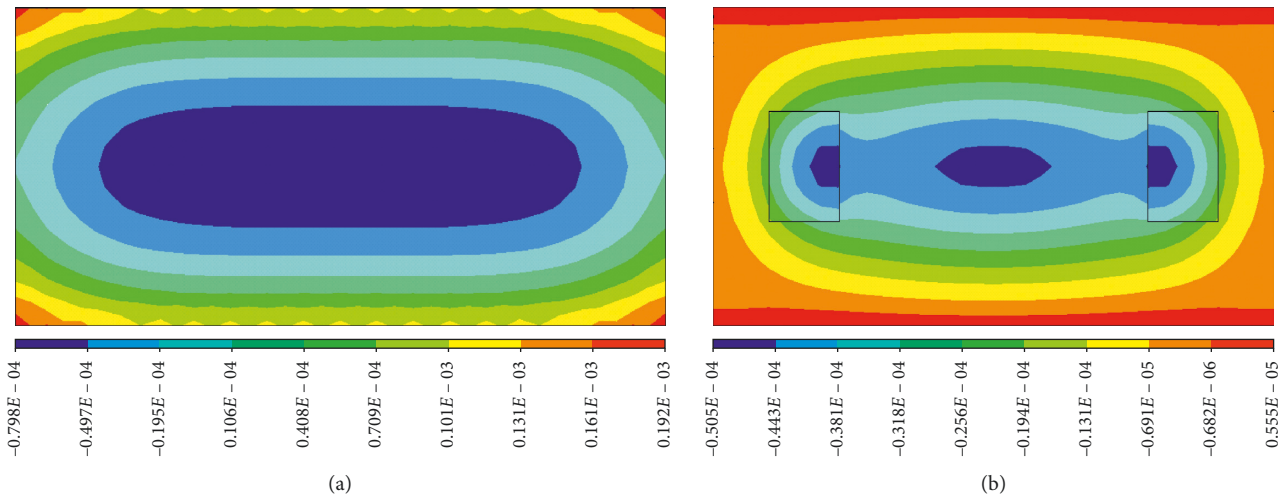

Figure 13: The deformation under −20°C/m temperature gradient. (a) Track slab. (b) Bed plate.

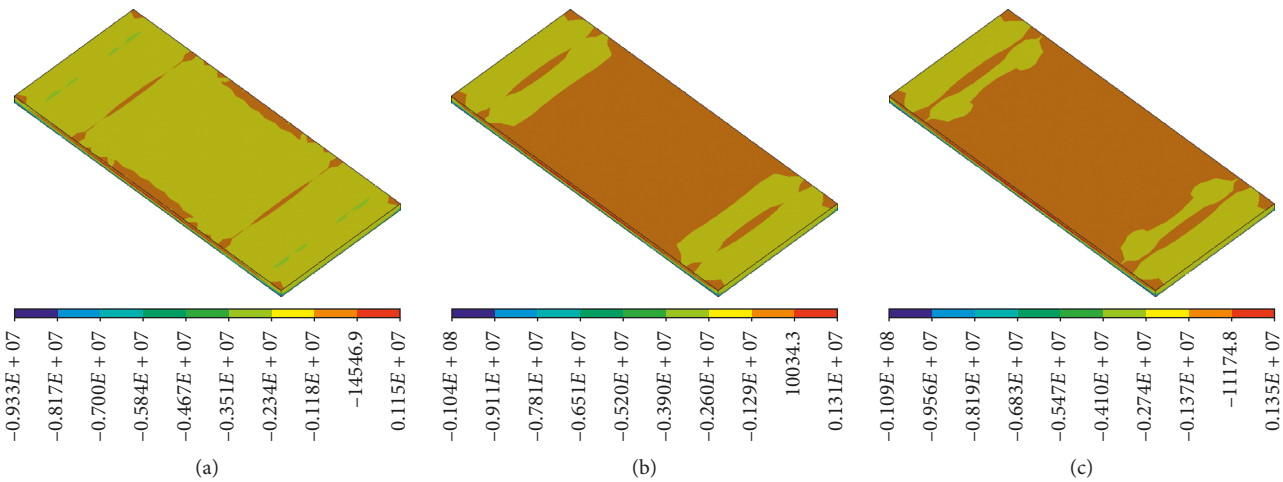

Figure 14: Longitudinal stress of the self-compacting concrete layer under condition 1. (a) $P = 50\%$. (b) $P = 90\%$. (c) $P = 95\%$.

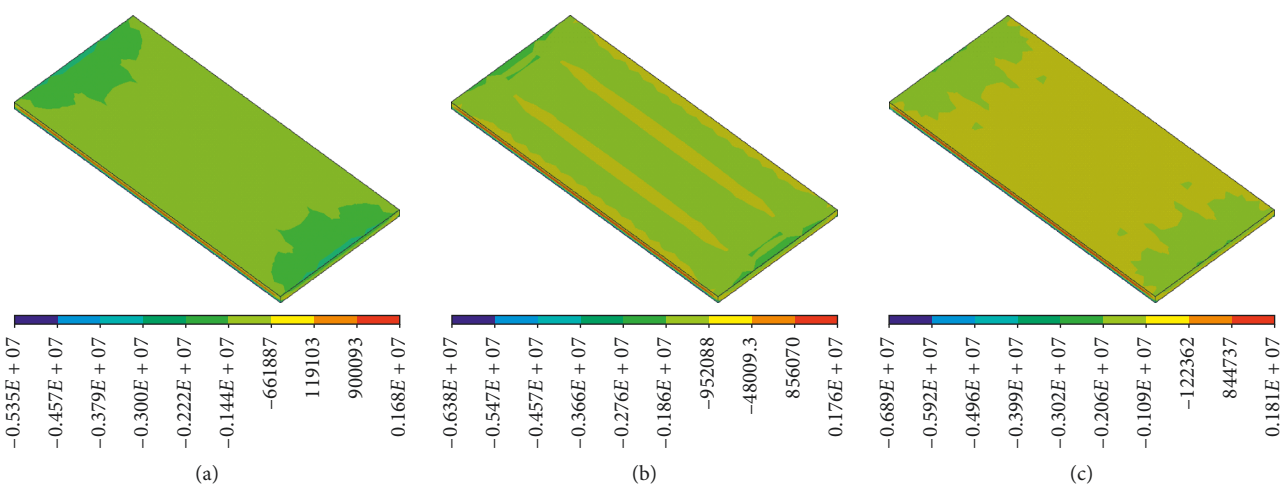

Figure 15: Transverse stress of the self-compacting concrete layer under condition 1. (a) $P = 50\%$. (b) $P = 90\%$. (c) $P = 95\%$.

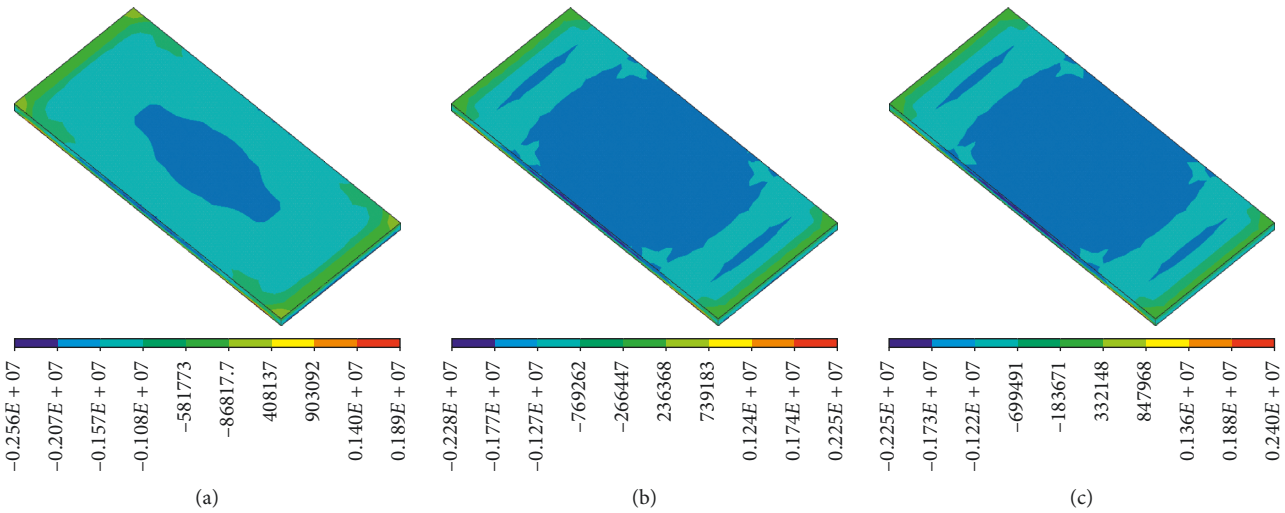

Figure 16: Longitudinal stress of the self-compacting concrete layer under condition 2. (a) $P = 50\%$. (b) $P = 90\%$. (c) $P = 95\%$.

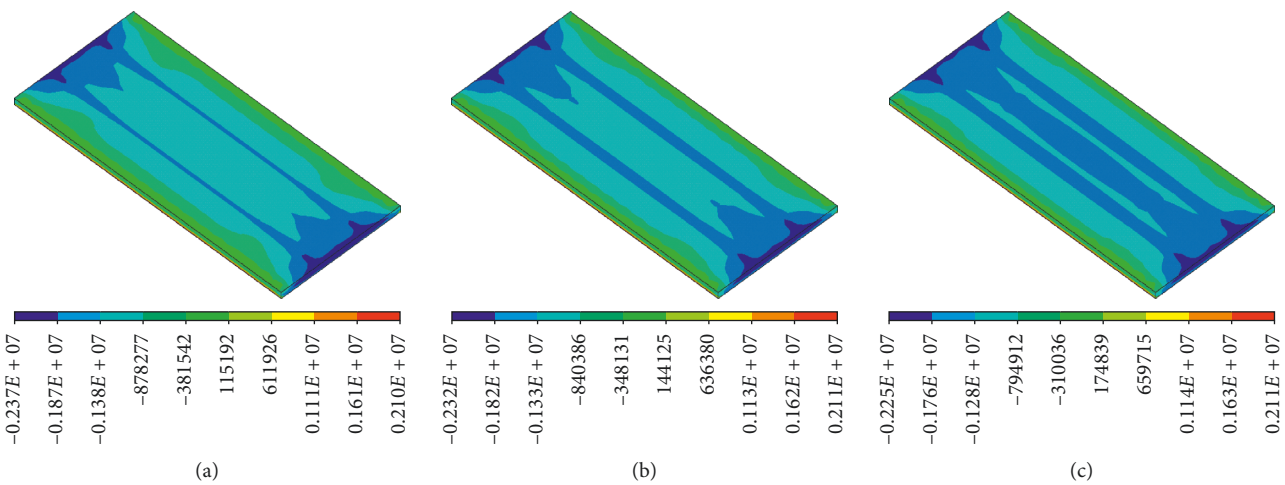

Figure 17: Transverse stress of the self-compacting concrete layer under condition 2. (a) $P = 50\%$. (b) $P = 90\%$. (c) $P = 95\%$.

Table 7: Maximum stress of the self-compacting concrete layer.

	Condition 1			Condition 2		
Safety probability (%)	$P = 50$	$P = 50$	$P = 90$	$P = 50$	$P = 90$	$P = 95$
Maximum longitudinal tensile stress (MPa)	1.15	1.31	1.35	1.89	2.25	2.40
Maximum longitudinal compressive stress (MPa)	9.33	10.4	10.9	2.56	2.38	2.25
Maximum transverse tensile stress (MPa)	1.68	1.76	1.81	2.10	2.11	2.11
Maximum transverse compressive stress (MPa)	5.35	6.38	6.89	2.37	2.32	2.25

tensile stress is located at both ends of the interface, and the maximum tangential stress is located at the edge of the interface. In addition, under condition 2, the stress of interface between track slab and self-compacting concrete layer is shown in Figures 24 and 25. The maximum normal tensile stress is located at the corner of the interface and the maximum tangential stress is located at the edge of the interface Figure 25. Furthermore, both normal and tangential maximum stress increases with the increase of the fractal value, as shown in Table 9.

6. Fatigue Performance of Key Structural Layers of Ballastless Track Structure

A relevant study [17] shows that the positive temperature gradient and the negative temperature gradient occur alternately, and the time of these two gradients in a day is basically the same. Therefore, it can be assumed that working conditions 1 and 2 all work 365 times in a year. The fatigue life under temperature can be calculated by using the following formula [23]:

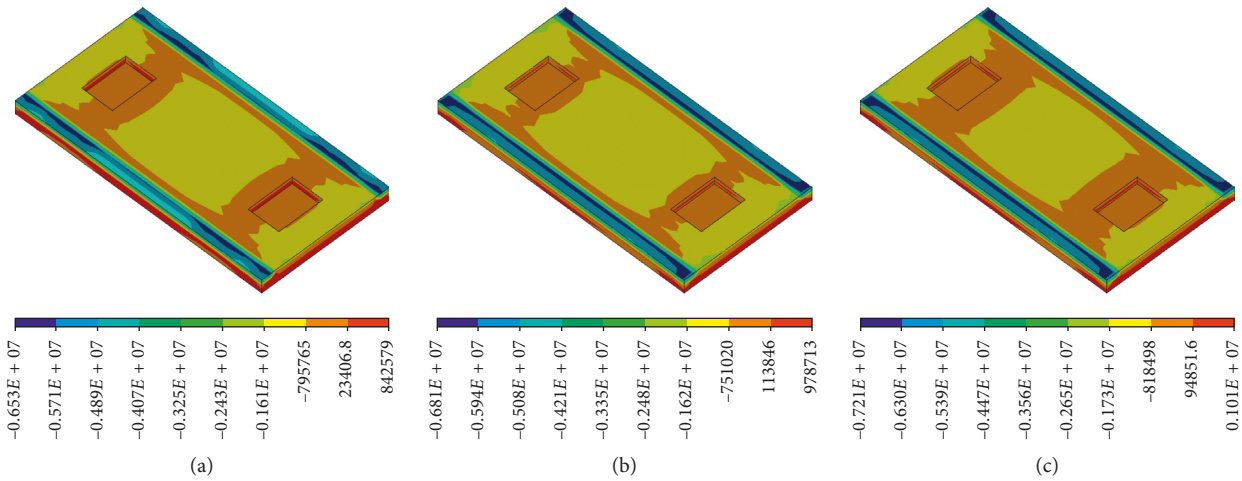

Figure 18: Longitudinal stress of the bed plate under condition 1. (a) $P = 50\%$. (b) $P = 90\%$. (c) $P = 95\%$.

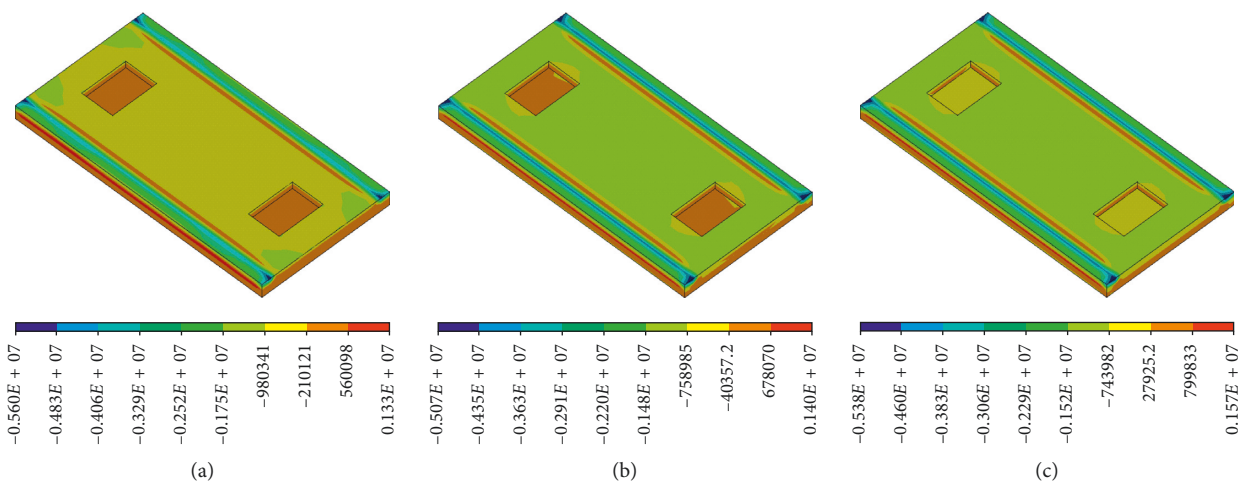

Figure 19: Transverse stress of the bed plate under condition 1. (a) $P = 50\%$. (b) $P = 90\%$. (c) $P = 95\%$.

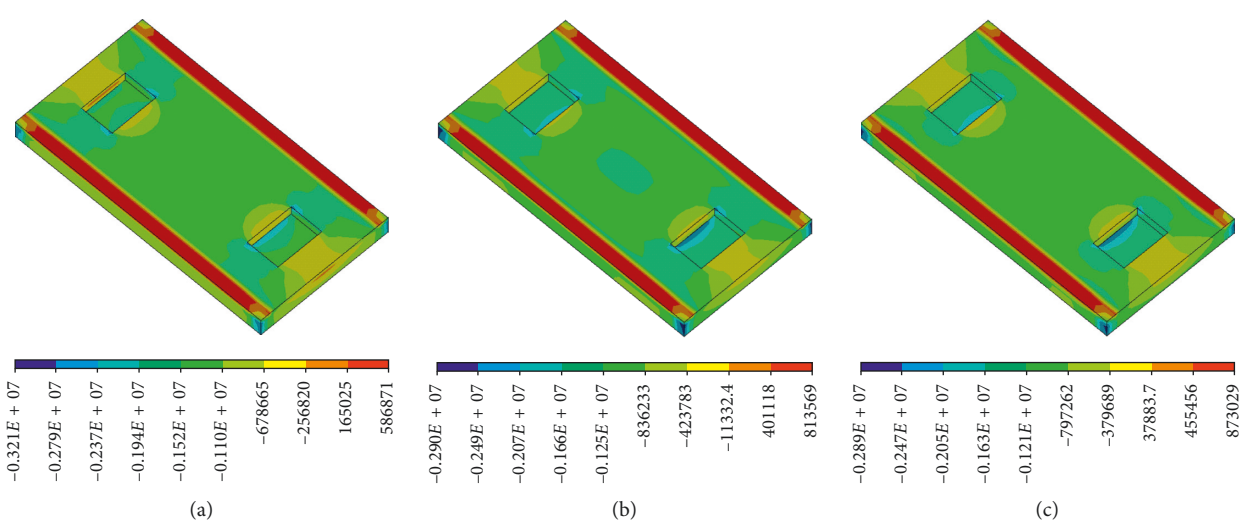

Figure 20: Longitudinal stress of the bed plate under condition 2. (a) $P = 50\%$. (b) $P = 90\%$. (c) $P = 95\%$.

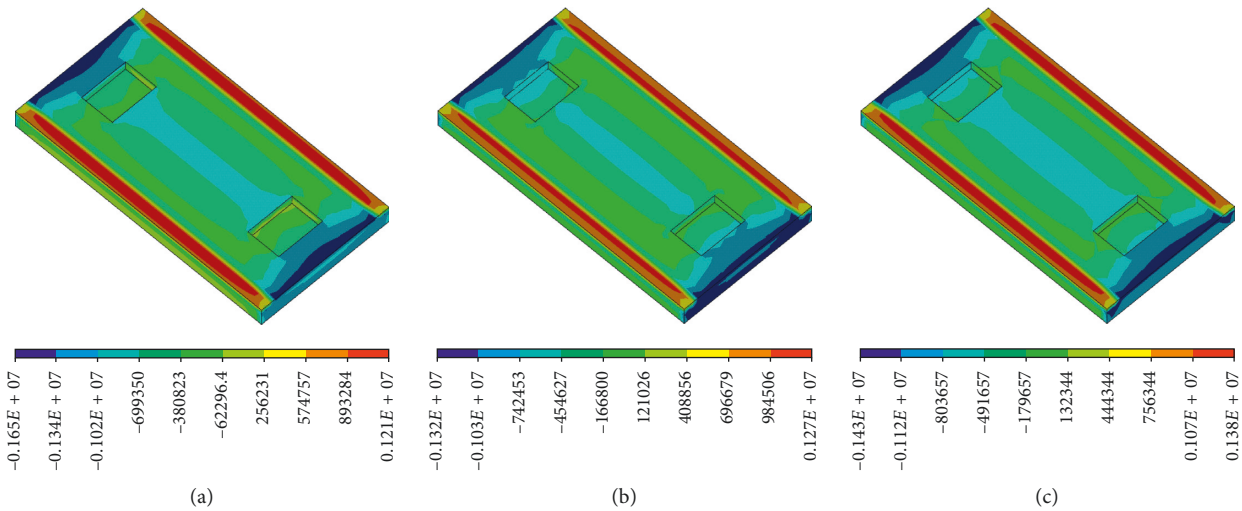

Figure 21: Transverse stress of the bed plate under condition 2. (a) $P = 50\%$. (b) $P = 90\%$. (c) $P = 95\%$.

Table 8: Maximum stress of the bed plate.

	Condition 1			Condition 2		
Safety probability (%)	$P = 50$	$P = 90$	$P = 95$	$P = 50$	$P = 90$	$P = 95$
Maximum longitudinal tensile stress (MPa)	0.84	0.98	1.01	0.59	0.81	0.87
Maximum longitudinal compressive stress (MPa)	6.53	6.81	7.21	3.21	2.90	2.89
Maximum transverse tensile stress (MPa)	1.33	1.40	1.57	1.21	1.27	1.38
Maximum transverse compressive stress (MPa)	5.60	5.07	5.38	1.65	1.32	1.43

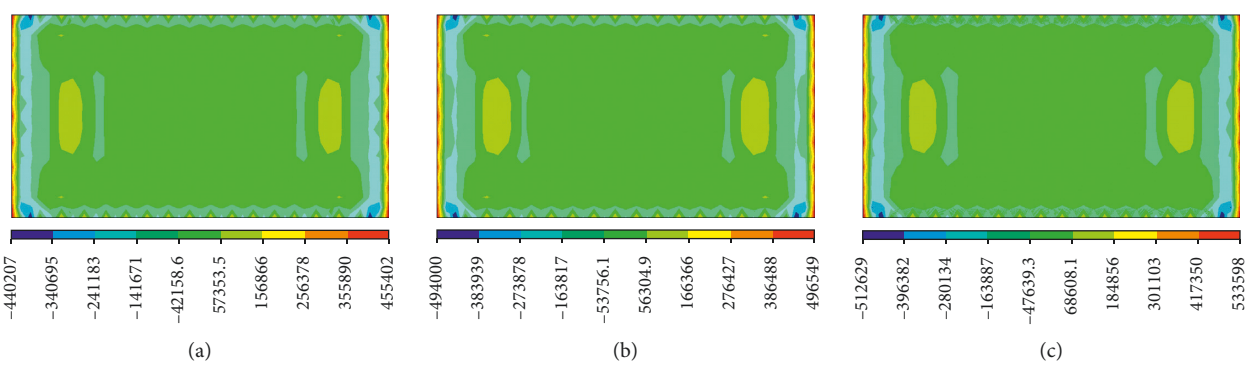

Figure 22: Normal stress of interface under condition 1. (a) $P = 50\%$. (b) $P = 90\%$. (c) $P = 95\%$.

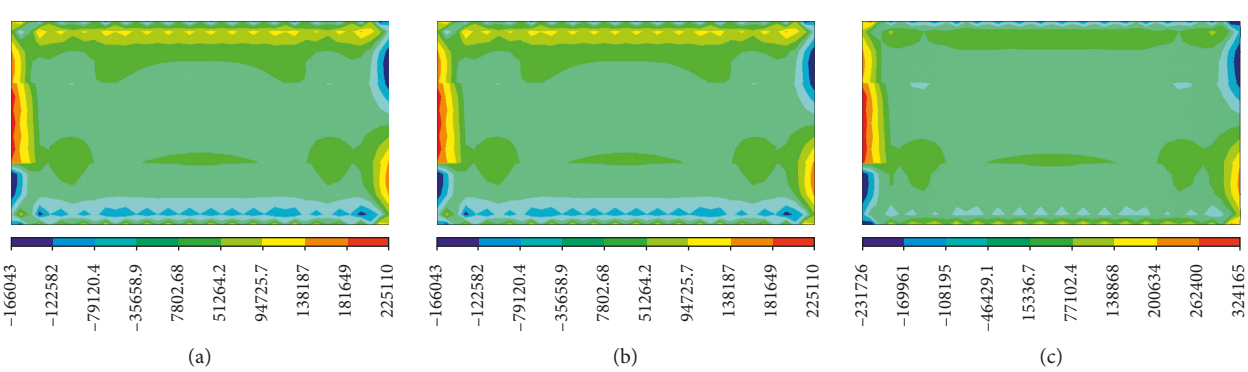

Figure 23: Tangential stress of interface under condition 1. (a) $P = 50\%$. (b) $P = 90\%$. (c) $P = 95\%$.

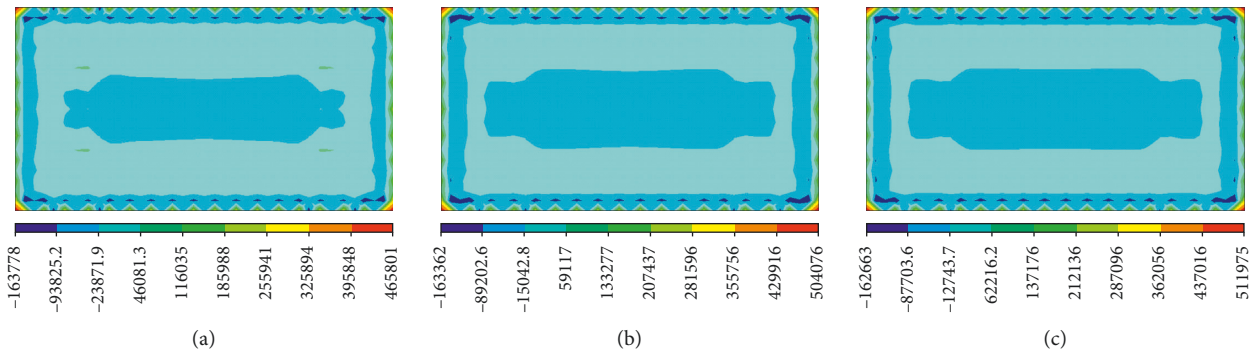

Figure 24: Normal stress of interface under condition 2. (a) $P = 50\%$. (b) $P = 90\%$. (c) $P = 95\%$.

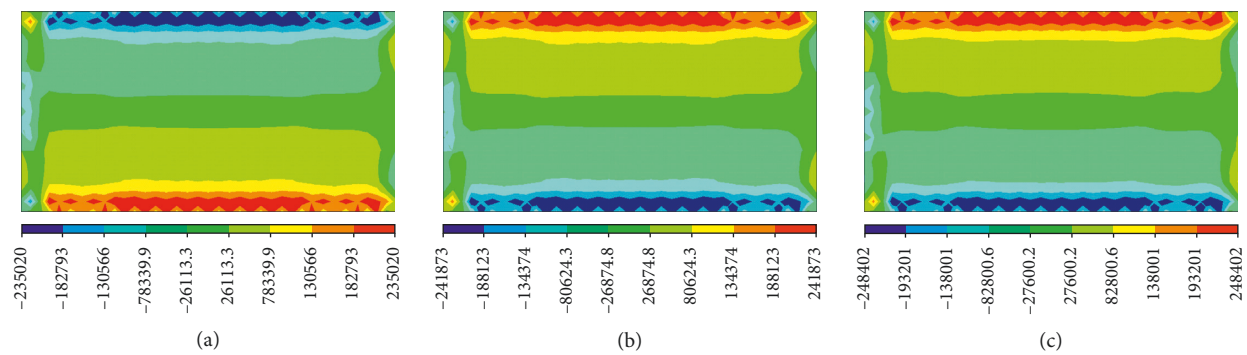

Figure 25: Tangential stress of interface under condition 2. (a) $P = 50\%$. (b) $P = 90\%$. (c) $P = 95\%$.

Table 9: Maximum stress of the interface.

	Condition 1			Condition 2		
Safety probability (%)	$P = 50$	$P = 90$	$P = 95$	$P = 50$	$P = 90$	$P = 95$
Maximum normal tensile stress (MPa)	0.45	0.50	0.53	0.47	0.50	0.51
Maximum normal compressive stress (MPa)	0.44	0.49	0.51	0.16	0.16	0.16
Maximum tangential tensile stress (MPa)	0.23	0.30	0.32	0.23	0.24	0.25
Maximum tangential compressive stress (MPa)	0.17	0.21	0.23	0.23	0.24	0.25

$$\log N^{\pm} = 14.7 - 13.5\frac{\sigma_{\max}^{\pm} - \sigma_{\min}^{\pm}}{f_{cu}^{\pm} - \sigma_{\min}^{\pm}}, \tag{13}$$

where $f_{cu}^{\pm}$ denotes the tensile (+) and compressive (−) strength of concrete. N denotes the fatigue life. $\sigma_{\max}$ and $\sigma_{\min}$ denote the maximum and minimum stress under temperature load.

Therefore, damage of the self-compacting concrete layer and bed plate in ballastless track structure can be calculated according to the following formula:

$$D = \frac{n}{N}, \tag{14}$$

where D denotes the damage variable. n denotes the fatigue load cyclic number.

Then, damage of the self-compacting concrete layer and bed plate under temperature load based on 95% safety probability after different service times is calculated, as shown in Tables 10 and 11. It can be seen that, for self-compacting concrete layer, damage under condition 2 accounts for 98.7% of the total damage which means condition 2 is the main damage factor. In addition, for bed plate, damage under condition 1 accounts for 88.5% of the

Table 10: Damage of the self-compacting concrete layer under temperature load after different service times.

	Damage under condition 1	Damage under condition 2	Total damage
1 year	1.15×10^{-4}	9.2×10^{-3}	9.32×10^{-3}
3 years	3.45×10^{-4}	2.76×10^{-2}	2.80×10^{-2}
5 years	5.75×10^{-4}	4.6×10^{-2}	4.66×10^{-2}
10 years	1.15×10^{-3}	9.2×10^{-2}	9.33×10^{-2}
20 years	2.30×10^{-3}	0.184	0.186
30 years	3.45×10^{-3}	0.276	0.280
40 years	4.60×10^{-3}	0.368	0.372
50 years	5.75×10^{-3}	0.460	0.466
60 years	6.90×10^{-3}	0.552	0.559

Table 11: Damage of the bed plate under temperature load after different service times.

	Damage under condition 1	Damage under condition 2	Total damage
1 year	5.16×10^{-5}	5.78×10^{-6}	5.83×10^{-5}
3 years	1.55×10^{-4}	1.73×10^{-5}	1.72×10^{-4}
5 years	2.58×10^{-4}	2.89×10^{-5}	2.87×10^{-4}
10 years	5.16×10^{-4}	5.78×10^{-5}	5.74×10^{-4}
20 years	1.03×10^{-3}	1.15×10^{-4}	1.15×10^{-3}
30 years	1.55×10^{-3}	1.73×10^{-4}	1.72×10^{-3}
40 years	2.06×10^{-3}	2.31×10^{-4}	2.29×10^{-3}
50 years	2.58×10^{-3}	2.89×10^{-4}	2.87×10^{-3}
60 years	3.10×10^{-3}	3.47×10^{-4}	3.45×10^{-3}

total damage which means condition 1 is the main damage factor.

7. Conclusion

In this work, through the statistical analysis of ten years' meteorological data, it has been found that the daily extreme values of monthly axial uniform temperature of CRTS III slab ballastless track structure obey normal distribution and the daily maximum temperature gradient obeys the extreme value I-type distribution.

In both conditions, the maximum tensile stress of the self-compacting concrete layer is located in the middle and edge of the slab bottom and the side of the slab. The maximum tensile stress of the base plate is located at the edge of the surface of the layer and the inner edge of the limiting groove. The interface normal tensile stress is located at the end and corner of the interface. Furthermore, maximum stress increases with the increase of the fractal value.

The main damage factors for self-compacting concrete layer and bed plate are the daily minimum value of axial uniform temperature is load combination of minimum axial temperature and maximum negative temperature gradient and load combination of maximum axial temperature and maximum positive temperature gradient.

Data Availability

The data used to support the findings of this study are included within the article.

Conflicts of Interest

The authors declare that they have no conflicts of interest.

Acknowledgments

This study was developed within the research project SY2016G001 funded by China Railway and U1434204 funded by the National Science Foundation of China, whose assistance is gratefully acknowledged.

References

[1] J. J. Wang, M. Wang, W. B. Liu, and Y. Zhao, "Technology of CRTS III; ballastless track system," *China Railway*, vol. 58, no. 8, pp. 10–15, 2017.

[2] S. R. Wang, "Study on temperature stress for ballastless track slab," Master's Dissertation, Southwest Jiaotong University, Chengdu, China, 2007.

[3] S. R. Wang, L. Sun, and Q. Y. Li, "Temperature measurement and temperature stress analysis of ballastless track slab," *Journal of railway engineering society*, vol. 26, no. 2, pp. 52–55, 2009.

[4] P. R. Zhao, X. Y. Liu, R. S. Yang et al., "Experimental study of temperature load determination method of Bi-block ballastless track," *Journal of the China Railway Society*, vol. 38, no. 1, pp. 92–97, 2016.

[5] L. X. Bi, P. R. Zhao, M. T. Xing et al., "Monitoring method of temperature field on bi-block ballastless track," *Journal of Railway Science and Engineering*, vol. 13, no. 9, pp. 1667–1673, 2016.

[6] Y. Liu, P. Chen, and G. T. Zhao, "Study on the characteristics of early temperature field of CRTS II slab ballastless track structure," *China Railway Science*, vol. 35, no. 1, pp. 1–9, 2016.

[7] P. R. Zhao, F. F. Deng, C. X. Ding et al., "Temperature gradient prediction of ballastless track in Chengdu region based on statistical analysis method," *Railway Engineering*, vol. 59, no. 5, pp. 43–46, 2016.

[8] L. Gao, M. X. You, H. Xiao et al., "Experimental study on relation between temperature distribution in CRTS II slab-type ballastless track and ambient temperature," *Railway Engineering*, vol. 59, no. 5, pp. 6–9, 2016.

[9] M. X. You, L. Gao, G. T. Zhao et al., "Analysis of monitoring test for slab-type ballastless track temperature field and temperature gradient," *Railway Engineering*, vol. 59, no. 5, pp. 1–5, 2016.

[10] Z. M. Ou, L. Sun, and Q. Q. Cheng, "Simplified calculation of temperature field in high-speed railway ballastless track structure," *Journal of Zhejiang University (Engineering Science)*, vol. 49, no. 03, pp. 482–487, 2015.

[11] Z. M. Ou, L. Sun, and Q. Q. Cheng, "Analysis on temperature field of ballastless track structure based on meteorological data," *Journal of the China Railway Society*, vol. 36, no. 11, pp. 106–112, 2014.

[12] G. L. Dai, M. Wang, J. B. Liang et al., "Study on temperature gradient of CRTS II twin-block ballastless track on bridge in summer," *Journal of Beijing Jiaotong University*, vol. 42, no. 1, pp. 40–46, 2018.

[13] G. L. Dai, H. T. Su, W. S. Liu et al., "Temperature distribution of longitudinally connected ballastless track on bridge in Summer," *Journal of Central South University (Science and Technology)*, vol. 48, no. 4, pp. 1073–1080, 2017.

[14] G. L. Dai, H. T. Su, B. Yan et al., "Nonlinear temperature distribution of longitudinal plate-type ballastless track in spring," *Journal of south China university of technology (Natural Science Edition)*, vol. 44, no. 2, pp. 20–25, 2016.

[15] G. L. Dai, H. T. Su, and B. Yan, "Experimental study on the vertical temperature gradient of longitudinally connected slab ballastless track on bridge in autumn," *Journal of Hunan university (Natural Science Edition)*, vol. 42, no. 3, pp. 94–99, 2015.

[16] G. L. Dai, X. G. Wen, and H. T. Su, "Study on horizontal and vertical temperature gradient of ballastless track on bridge in cold season," *Journal of Huazhong University of Science and Technology (Natural Science Edition)*, vol. 43, no. 7, pp. 1–5, 2015.

[17] W. B. Liu, J. J. Wang, Q. L. Yang et al., "Experimental study on temperature gradient of CRTSIII slab ballastless track in high speed railway," *Railway Engineering*, no. 3, pp. 103–106, 2015.

[18] Chinese National Standards, *Load Codes for Building Structures*, Ministry of Housing and Urban-Rural Development of the People's Republic of China, Beijing, China, 2012.
[19] Chinese National Standards, *Code for Design of High Speed Railway*, Ministry of Railways of the People's Republic of China, China Railway Publishing House, Beijing, China, 2014.
[20] Z. Yu, Y. Xie, Z. Shan, and X. Li, "Fatigue performance of CRTS III slab ballastless track structure un-der High-speed train load based on concrete fatigue damage constitu-tive law," *Journal of Advanced Concrete Technology*, vol. 16, no. 5, pp. 233–249, 2018.
[21] C. Jin, "Experimental study on the cooperative performance of track slab-self compacting concrete layer in the CRTS III slab track system," Master's Dissertation, Central South University, Changsha, China, 2016.
[22] C. He, "Research on the performance of CRTSIII slab ballastless track structure under the action of temperature-train load," Master's Dissertation, Central South University, Changsha, China, 2017.
[23] *Research on Fatigue Reliability Checking Method of Concrete Flexural Members. Concrete Fatigue Group*, Beijing, China, 1994.